Applied Physics A (2019) 125:812
https://doi.org/10.1007/s00339-019-3106-7

Applied Physics A
Materials Science & Processing

Fabrication of gold nanorod–zinc oxide nanocomposite on gap-fingered integrated interdigitated aluminum electrodes and their response to electrolytes

Hussaini Adam[1] · Subash C. B. Gopinath[1,2] · M. K. Md Arshad[1,3] · Santheraleka Ramanathan[1] · Thanganadar Ashokkumar[4] · Mohammad Isa Ahmad Azan[1] · Tijjani Adam[5] · Uda Hashim[1]

Received: 17 July 2019 / Accepted: 25 October 2019

Abstract

This study describes the fabrication of three different gap-fingered aluminum-interdigitated electrodes (AlIDEs) on the silicon substrate based on photolithographic method, followed by integration of the gold nanorod–zinc oxide nanocomposite. The IDE masks were designed using AutoCAD software with the gaps of 10, 20, and 30 µm for design 1, 2, and 3, respectively. The morphological and electrical characterizations were subsequently performed using 3D-nanoprofiler, atomic force microscopy, high-power microscopy (HPM), scanning electron microscopy (SEM), and I–V. Validation of the fabricated surfaces (AlIDEs with/without gold nanorod–zinc oxide nanocomposite) against the electrolytes was performed at different pHs which are ranging from 1 to 12. SEM revealed the following gaps, 18.4, 20, and 40.5 µm for bare 1, 2, and 3, respectively. The measurements on I–V for bare AlIDEs indicated the electrolyte influences at different pH solutions, which were almost similar in terms of current variations except at highly acidic and alkaline. AlIDEs were well fabricated and the smaller the gap displayed the better the sensitivity, hence device 1 AlIDE has a good performance. Using different pH solutions which ranging from pH 1–12, before and after AlIDEs were coated with zinc oxide and gold nanorod. The responses of the devices were similar, fluctuating from highly acidic region to highly alkaline region in the cases of AlIDEs bare 1 and 3. Bare 2 AlIDE displayed similar responses with the AlIDE that was deposited with gold nanorod. With these results, we can conclude that deposition of gold nanorod on the device brought about the orderly response to the different pH and with the increment from acidic to alkaline increases, the proportional changes with the current were noticed.

1 Introduction

In 1967, a sensor was developed with the immobilized antibody and considered as the initiation of solid substrate for the sensing application, proposed by Catt and Niall [1]. Advancement of technologies in the past have steered the growth of various analytical devices to monitor different analytes [2]. Nanotechnology is a promising field of science, which includes synthesis and development of different nanomaterials and nanodevices [3]. Development of two-dimensional layered nanomaterials have attracted a great demand due to their fascinating physiochemical properties with the excellent physical, optical, and electrical characteristics that have been emerged from the quantum size effect on ultrathin structure [4]. Two-dimensional nanomaterial such as graphene with atomic thicknesses has fascinated a strong scientific interest because of its good optical, electronic, thermal, mechanical, and electrochemical properties [5]. On the other hand, nanobiosensor is one of the innovative

Electronic supplementary material The online version of this article (https://doi.org/10.1007/s00339-019-3106-7) contains supplementary material, which is available to authorized users.

✉ Subash C. B. Gopinath
subash@unimap.edu.my

1 Institute of Nano Electronic Engineering, Universiti Malaysia Perlis, 01000 Kangar, Perlis, Malaysia

2 School of Bioprocess Engineering, Universiti Malaysia Perlis, 02600 Arau, Perlis, Malaysia

3 School of Microelectronic Engineering, Universiti Malaysia Perlis, Pauh Putra, 02600 Arau, Perlis, Malaysia

4 RSET and RSIT, Assam Royal Global University, Guwahati, Assam 781035, India

5 Faculty of Technology, Universiti Malaysia Perlis, Kampus Uniciti Alam Sg. Chuchuh, 02100 Padang Besar (U), Perlis, Malaysia

Published online: 06 November 2019

systems converting the biological interactions into the signals that are measurable [6].

The quality of biosensors is primarily recognized by the specificity along the potential of the transducer and the reliability in analyzing the interactions of biomolecules to achieve the contemporary quality assurance [7]. For the detection of analytes, a biosensor must possess characteristics such as linearity, sensitivity, selectivity, reproducibility, and stability [8]. Biosensor with a high sensitivity is capable of detecting diseases at their early states and significantly proving the chance of possible life-saving detection and intervention [9]. As a result of the advancement of fields such as nanotechnology and nanoscience, nanomaterial-based electrochemical for signal amplification is a promising tool in improving the high performance of biosensors [10]. In addition, biosensing devices are useful to determine the concentration of substances at the biologically relevant parameters [11].

To recognize the quality of a biosensor, it is important to highlight the relationship between solid-state and sensitivity properties. The sensing process is strongly related to the surface reactions [12]. High surface areas can provide large reaction contact area between the sensing materials and target gases. Porous structure with high surface areas seems to be the standard structure of metal oxide gas sensor layers. It is also showed that nanoscale grain size is useful to enhance the sensitivity [13]. The results demonstrated the importance of the achieving of a large effective surface area for improving sensitivity of sensor [14]. Relationship between solid structure and sensitivity properties was reported based on facile, solid-state reaction assisted synthesis of sodium niobiate. The sensor showed a high sensitivity and excellent reproducibility and selectivity across various possible interfering species [15].

Furthermore, biosensor is an important analytical device that has fascinated numerous interests as a result of their wide range of applications in diagnosis and biomedicine [16]. This can be the results of biosensing devices, which offer vital benefits, such as small sizes, quicker response, and their development at low price. Even though biosensors are extensively investigated in research, they have limited commercialization as a result of the complexity in detecting impedance, biomolecular immobilization stability, suitability with smaller sized analytes, and nonspecific absorption [17]. Apart from these, another major task applicable to biosensor is design and development depending on the understanding of the relationship between the reactivity and the surface molecules. By comprehending the process that governing the response for the biosensor, will lead to a development of electroanalytical devices with greater selectivity and sensitivity [18–20].

Currently, biosensors perpetually play important roles in various fields of engineering and science and have opened a new scope for the detection of analytes such as drug, blood, and metabolites [21]. Several studies have been done for the development of new sensing materials that are able to comply with important criteria, such as low cost, high reliability, greater sensitivity, and a quick response [22]. These requirements call for the reduction of device sizes since the size miniaturization will enhance the performance and more functions in a small set can be integrated. Along with the study line, a biosensor has been developed as a dielectric interdigitated electrode (IDE), having a pivotal role in the medical diagnosis [18]. The operation of these biosensors can be in faradaic or non-faradaic process [23]. Faradaic operation of a biosensor is based on the flow of current when electrons are transferred from one electrode to another. The operation of a biosensor in non-faradaic form occurs when the current flows through a capacitive electrode. A biosensor that operates in faradaic way is based on electrochemical impedance and measuring the electron transfer resistance. The non-faradaic operation of a biosensor is as a result of change in capacitance between interdigitated electrodes for the indication of molecular binding/interaction on the surface of the electrodes [18, 24–26].

IDE can be a capacitance or impedance sensing for the label-free and the sensitive detection. There are several advantages of IDE, such as cells can be cultured and measured with label-free assays of electrical [14]. Furthermore, the generation of hybrid nanostructures has been proven as a potential method of developing a biosensor with high performance [27]. In the current research, aluminum is selected for the fabrication of IDEs because of its low price and the most common electrode in use [22]. Aluminum-interdigitated electrodes (AlIDEs) consists of two independently vivid interdigitated in the form of comb-finger structure have commonly been recommended as a biosensor that showed the potential to develop a higher sensitivity than the conventional parallel electrodes. Furthermore, zinc oxide was embedded with different gold nanorods of three different sizes and coated on AlIDEs as these are playing major roles in the biosensor development [28]. With this development, by testing the influence of electrolytes at various pH solutions on the substrate of the IDE, a biosensor can be simply evaluated for the high-performance bioanalysis. This research initially tested the influence of electrolytes on the silicon-embedded aluminum electrode surface. Similar evaluation was done on the impregnated gold nanorod–zinc oxide composite. To support further, the physical, chemical, and electrical characteristics of the AlIDEs were studied.

2 Materials and methods

2.1 Chemicals, reagents, and instruments

The pH buffer solutions with different range were purchased from HANNA Instruments with the accuracy of pH ± 0.01

used for the pH scouting. Gold nanorod with different sizes were purchased from Nanocs, USA. Three different sized gold nanorods of 550, 700, and 980 nm were used and stored at 4 °C. Acetone, aluminum oxide, resists developer (RD6), and positive photoresist (PR1-3000A) were bought from Futurrex, Inc. Other chemicals utilized in this study were of analytical grade obtained from Mallinckrodt Baker and used without any further purification. The AlIDEs mask was designed using AutoCAD Software with miniaturizations, after that, the design was transferred to a commercial chrome mask that was prepared by Silterra (M) Sdn Bhd, Malaysia. High-power microscopy (HPM), scanning electron microscopy (SEM), 3D nanoprofilor, and atomic force microscopy (AFM) were used for the physical and morphological characterization of bare AlIDEs and with gold nanorod–zinc oxide nanocomposite. SEM was used for the characterization of the AlIDEs surface operating at 20 kV with 7000 magnification at room temperature [29]. I–V characterization measurements were done using Keithley 2450 assisted with Kickstart software and probe station and the testing of the three fabricated AlIDEs was carried out by applying drops of different pH ionic solutions to the desired surfaces at room temperature.

3 Fabrication of aluminum-interdigitated electrodes (AlIDEs)

Three different interdigitated electrodes were fabricated by the conventional photolithographic process as followed previously [23]. To achieve a better sensitivity with the electrochemical detection of affinity-based biomolecular interactions, electrodes with a significantly conductive aluminum were preferred. The designing of the photomasks for AlIDE was done using the AutoCAD software. The schematic designs of IDE consist of 20 finger electrodes with different lengths and gap sizes. After designing the IDEs, chrome mask was used to be printed. The fabrication of the devices was conducted on silicon wafer as the base material. First, the silicon wafer was thoroughly cleaned using RCA1, RCA2, and deionized water solutions for removing any impurity on the surface of the substrate, followed by the thermal oxidation at the temperature 950 °C to obtain a better quality of 1000 nm thick silicon dioxide layer. Moreover, 15 nm thick layer of aluminum was deposited which acts as an adhesive layer. The initial step of the photolithographic process revealed the pads, connector, and digits of two electrodes through Ultra-violet via the photomask on to the soft photoresist. The development of the pattern occurred in the soft mask and transferred on to the hard mask based on the etching process, and then finally the soft photoresist was stripped. Patterning of AlIDEs was conducted via deep-reactive ion-etching process and the produced AlIDEs with virtually vertical partitions. At the end, the photoresist layer was stripped and these processes resulted in a symmetrical IDE array with 20 digits from each side. Similar conventional photolithographic process was followed to fabricate three different types of AlIDEs.

4 Gold nanorod–zinc oxide nanocomposite deposition

Gold nanorod–zinc oxide nanocomposite deposition on the AlIDE is crucial and the fundamental studies on such modified electrodes have been performed to obtain a better comprehension of the nature of charge transfer and charge transport process inside the thin films [30]. Nanostructured composite materials coupled with impedimetric/voltammetry sensing offers a feasible solution [31]. In biosensors, gold nanorod and zinc oxide play crucial roles in term of stability, sensitivity, biocompatibility, and low cost. One of the most significant advantages of this deposition is the ability to control the size and distribution of nanoparticles by simply varying potential, time, or solution concentration [32]. Hence, gold nanomaterial can be deposited in a short period at a high growth rate, their deposition can be deliberately localized at the electrode surfaces with a minimal material waste [32]. IDE design is one of the device architectures in biosensor for label free, stability, and sensitivity.

5 Electric measurements: pH scouting

The measurements of I–V were performed using picoammeter/voltage source with a probe station. Before the measurement with different pH solutions on the prepared microgaps, primarily, cleaning was done using acetone followed by deionized water. After that, pH solutions from 1 to 12 have been tested by dropping gently on the entire sensing surfaces of the microgaps. The changes in current were observed and measured to see the influence of the electrolytes with different pH solutions on the sensing surface.

6 Results and discussion

The application of gold nanorod and zinc oxide in biosensors is important in term of stability, sensitivity, and biocompatibility [33]. Interdigitated electrode (IDE) design is one of the device architectures in biosensor for label free, stability, and sensitivity [34]. Voltammetry biosensors are the most promising systems for the biomedical point-of-care testing because of their non-complex nature and label-free operation [35]. The IDE is operating with the voltammetry could be fabricated using gold, platinum, titanium, chromium, carbon, indium, and tin oxide, although the most generally used materials are silicon oxide and aluminum oxide [36]. The method of selecting electrode materials for the fabrication of IDE is depending on the intended purpose, the existence of ionic species, the inertness to the environment, and the suitability to the fabrication method [35]. Electrode material such as carbon has a broader potential window compared to the metal electrodes [37]. These features are predictable to improve the sensitivity of electrochemical reactions for sensing biomolecules. However, carbon compounds have a high resistivity because of the contact resistance between carbon particles that makes them to develop high internal series resistance [38].

In the current project, three AlIDEs were fabricated as voltammetry electrochemical sensors for monitoring the influence of pH solutions. The designs were drawn based on AutoCAD with the specific dimensions (Fig. 1). Fabrication of the sensing IDE surfaces was carried out by the standard UV-photolithography approaches [39] (Fig. 2). Before proceeding for pH scouting to reveal the influence of electrolytes, the designs were morphologically characterized through the imaging processes.

The fabricated AlIDE surfaces were characterized using 3D nanoprofilometer, AFM, HPM, and, SEM for testing the formation of intact AlIDEs surfaces. Furthermore, gold nanorod and zinc oxide nanocomposite was deposited on AlIDE using spin coater and hot plate and tested at different pH solutions. Each device was placed on a spin coater for drying before pre-heated at a temperature of 80 °C for 10 min. Structural and elemental characterizations of the gold nanorod–zinc oxide-deposited AlIDE were carried out using SEM, AFM, 3D profilometer, and HPM and further electrical characterization was conducted using I–V characterization.

In the present research, nanoscaled gold nanorod and aluminum-interdigitated electrodes (AlIDE) were characterized. The analysis of AlIDE under SEM revealed the precision of the fabricated devices with microscale gaps for gold-nanorod deposition. Nanoscale sizes of gold nanorod were characterized and deposited on AlIDE. Although the gap sizes are originally designed for AlIDE fabrication, the deposition of gold nanorod–zinc oxide nanocomposite enables the transformation of sensing surface into nanoscale from microscale. The benefit of a greater surface area and improved reactivity in nanostructured materials help to create better catalytic actions and support the functionalization of biomolecules on nanoscaled material surfaces for the applications are ranging from drug delivery to more affordable modes of producing and storing energy. The transformation of microscaled to nanoscaled gap sizes of devices with the deposition of nanomaterials and nanocomposites also eliminates the difficulties faced in fabricating nanoscaled devices with low-yield fabricating steps [40]. Therefore, the author emphasizes the term 'nanoscale' in the title of this article, instead of microscale.

6.1 Surface area characterization of AlIDEs

6.1.1 3D-profilometer images

3D nanoprofilometer was used for three-dimensional analysis of grains between AlIDE finger electrodes. This

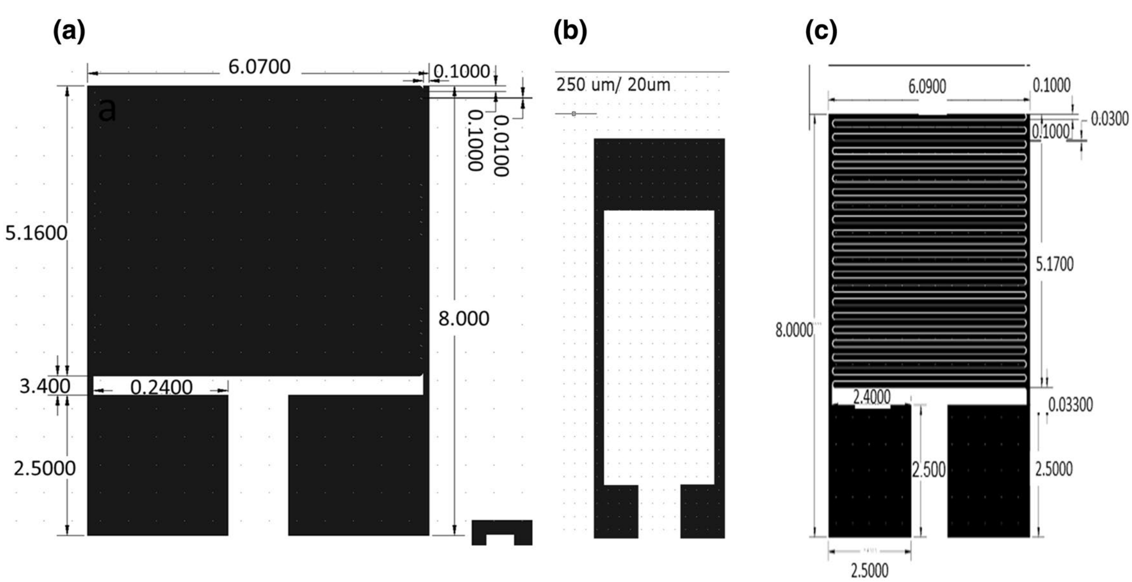

Fig. 1 AutoCAD designs: the IDEs with three different patterns including finger-shape, square shape, and connector's parts were designed with AutoCAD software from conceptual design. **a** Pattern 1; **b** Pattern 2; **c** Pattern 3

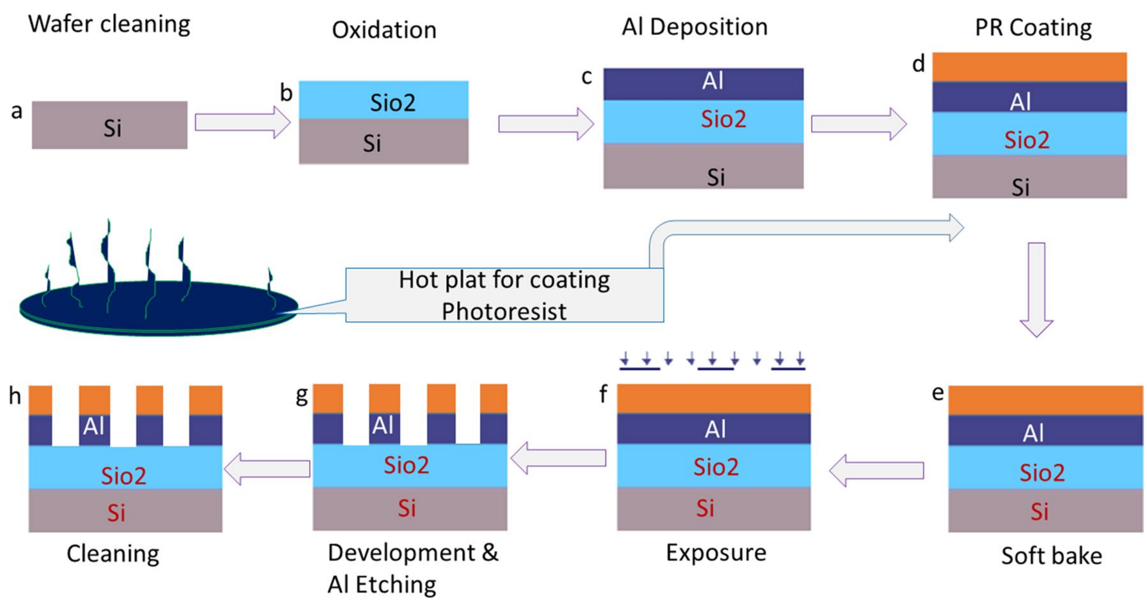

Fig. 2 Step-by-step fabrication process of the Aluminum-interdigitated electrode: The process started by rinsing with distilled water in order prevent redeposition. **a** wafer cleaning; **b** silicon oxide growth; **c** Aluminum deposition; **d** photoresist coating; **e** soft bake; **f** exposure; **g** development and Al Etching; **h** stripping of the photoresist and cleaning with acetone

scan was done based on a single point, a line scan and 3D scan. A profiler was also used to measure the surface profile for analyzing its roughness to differentiate between bare and the deposited surfaces. Based on the images captured by 3D profilometer of the finger electrodes in the active surface areas of the AIIDEs, they shows that the AIIDEs were well deposited with zinc oxide and different gold nanorod sizes. The experimental results show significant improvement in 3D-detector performance as the finger electrodes can be seen clearly on all the three types of the bare AIIDEs images. 3D bare images of AIIDEs with finger electrodes of different views are shown in Figure S1. Each type of gold nanorods and zinc oxide can be differentiated clearly by the physical appearances of the 3D images of AIIDEs (Fig. 3). Multiple formations of colors indicate the differences in the height from top to down. Sharp and smooth finger electrode edges are able to be seen in the images. Therefore, it can be said that the etching process has reached its required level of the developmental processes. The images of profiler before 3D analysis on AIIDEs with and without zinc oxide and gold nanorods show that the AIIDEs were well fabricated without shortcomings. The coating of the gold nanorods and zinc oxide can well be seen on the surfaces of the AIIDEs as scratches for both gold nanorod and zinc oxide and which indicated that the deposition was successful on the desired surfaces of the AIIDEs.

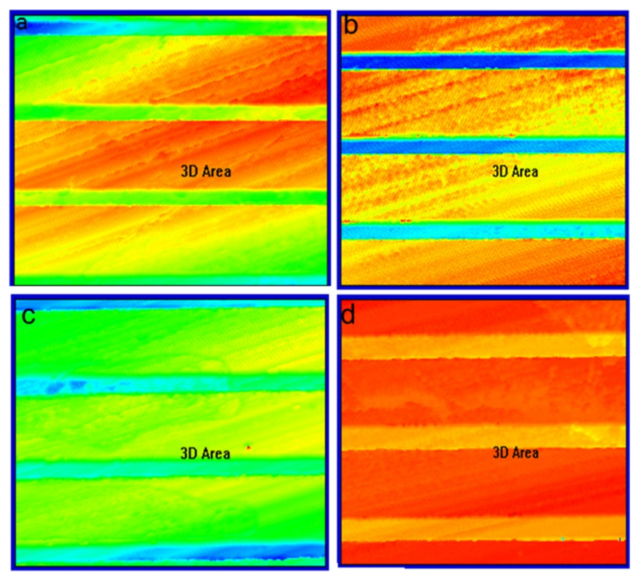

Fig. 3 Viewing and analyzing 3D images of AIIDEs coated with zinc oxide and different gold nanorod sizes using 3D Profilometer: **a** 3D image of AIIDE after coated with Zinc oxide, **b** 3D image of AIIDE after coated with gold nanorod size of 550 nm, **c** 3D image of AIIDE after coated with gold nanorod size of 700 nm, **d** 3D image of AIIDE after coated with gold nanorod size of 980 nm

6.1.2 Atomic force microscope (AFM)

AFM was used for imaging at the nanometer scale, uses a cantilever with a sharp probe that scans the surface of the sample. After AIIDEs fabrication by a standard

UV-photolithography process, AFM was used to image three different bare AlIDEs and after coated with gold nanorod and zinc oxide to show its structures and the functionalities. AlIDE sensors were imaged using AFM operating in the tapping mode. The measurements were performed on AlIDEs without zinc oxide and gold nanorods and with zinc oxide and gold nanorods of different sizes coated on the AlIDEs active surfaces with the resonant frequency of 300 kHz. Images were determined from a total of seven AFM images and characterization of the AlIDEs structure is depicting the uneven electrode edges due to the lift-off process. The images of the three different bare AlIDEs show the oxide layers (white grains) and aluminum layers (brown compartments), whereas images of the AlIDEs pattern on the coated gold nanorods and zinc oxide indicate the crystallized quartzite structures (Fig. 4).

6.1.3 High-power microscope (HPM)

Furthermore, the surface areas of the AlIDE patterns were characterized by HPM for the identification of the finger electrodes and the gaps between the finger electrodes. HPM images have indicated that the active surface areas of the AlIDEs have no distortions. The surface characterization using HPM revealed the finger electrode lengths and gap sizes of AlIDEs, such as 7.65, 13.11, and 32.67 μm of bare 1, 2, and 3 devices, respectively. Gap size of bare 1 device is smaller than the gap sizes bare 2 and 3 devices indicating that bare 1 device has the better sensitivity as compared to bare 2 and 3 devices as the smaller gap gives the better sensitivity. The images of AlIDEs captured using HPM of three different bare devices (Fig. 5). Images of AlIDEs captured using HPM (Figure S2).

6.1.4 Scanning electron microscope (SEM)

The surface characterization of the finger electrode pattern images of AlIDEs was performed using SEM and produced the images that contain the information about the surface topography of the AlIDEs. As indicated by SEM images, the sharp edges between finger electrodes of AlIDEs have validated that the sensor surfaces are well fabricated without defects. The images of AlIDEs produced by SEM before coating with gold nanorod and zinc oxide (bare) and after coated with gold nanorod and zinc oxide revealed that gold nanorod and zinc oxide were successfully deposited, as indicated by the white dotted spots on the surface of AlIDEs represent the gold nanorods and the dark circled spot on the surface of the AlIDEs represents zinc oxide (Fig. 6). SEM measurement on gap sizes and finger electrode lengths indicated the well characterization and fabrication of the AIIDEs. The images AIIDEs of the

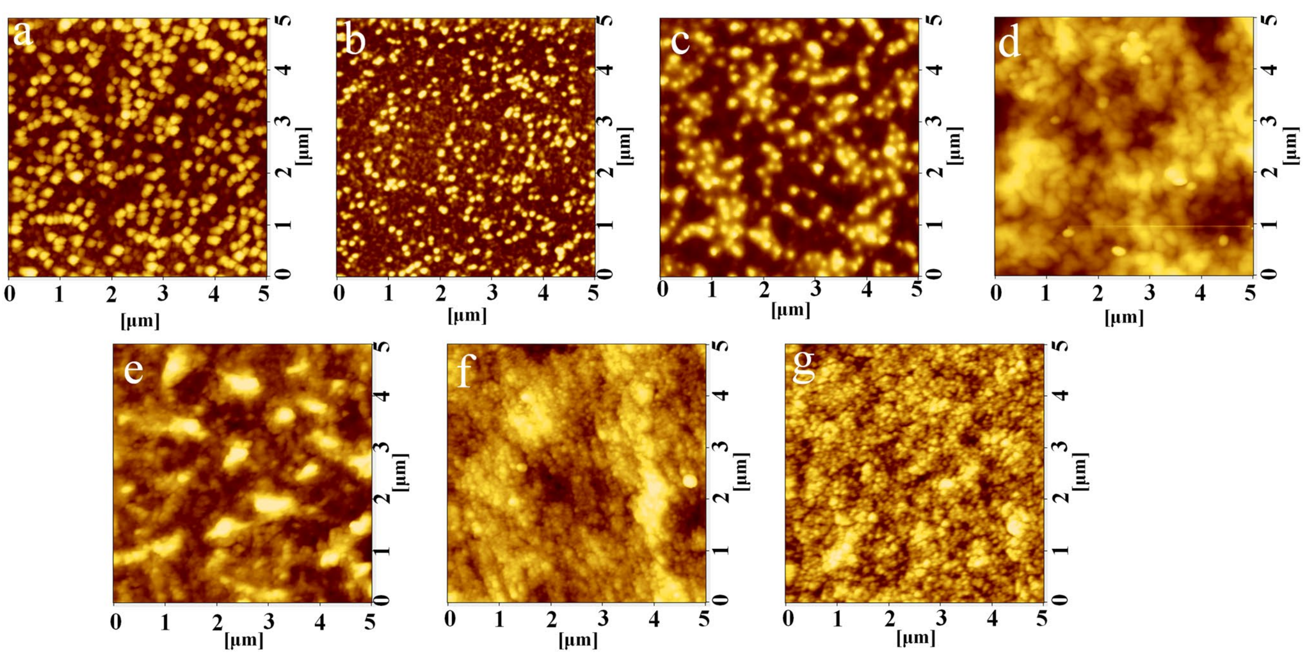

Fig. 4 After AlIDE fabrication by standard UV-photolithography process, AFM was used to captured the images of the AlIDEs with and without zinc oxide and gold nanorods: **a** AFM image of bare 1, **b** AFM image of bare 2, **c** AFM image of bare 3, **d** AFM image of AlIDE after coated with zinc oxide, **e** AFM image of AlIDE after coated with gold nanorod of size 550 nm, **f** AFM image of AlIDE after coated with gold nanorod of size 700 nm, **g** AFM image of AlIDE after coated with gold nanorod of size 980 nm

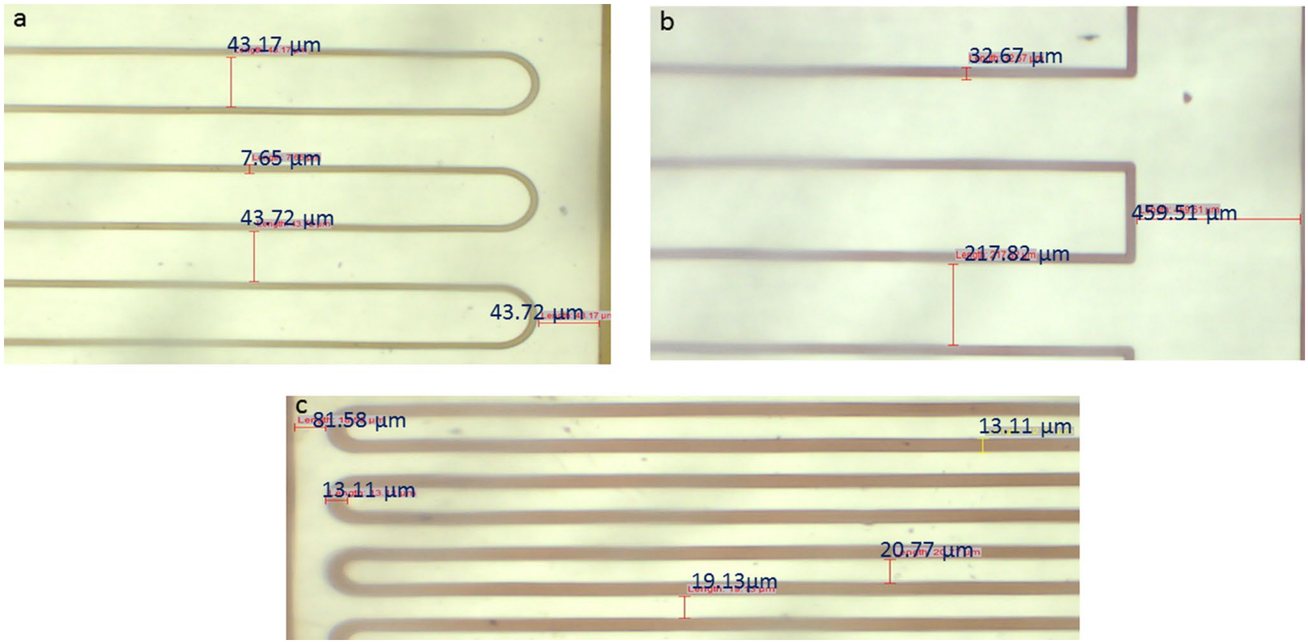

Fig. 5 The images of AlIDEs with gap and finger electrode sizes were determined using high-power microscope (HPM): **a** bare 1 HPM image, **b** bare 2 HPM image, **c** bare 3 HPM image

SEM for both left and right finger electrodes on the surface displayed the surface topographies as the gap sizes and the finger electrode lengths can be clearly seen (Figure S3). It can be apparently seen that the finger electrodes of the AlIDEs were well fabricated in micron scales with nice sharps and patterns.

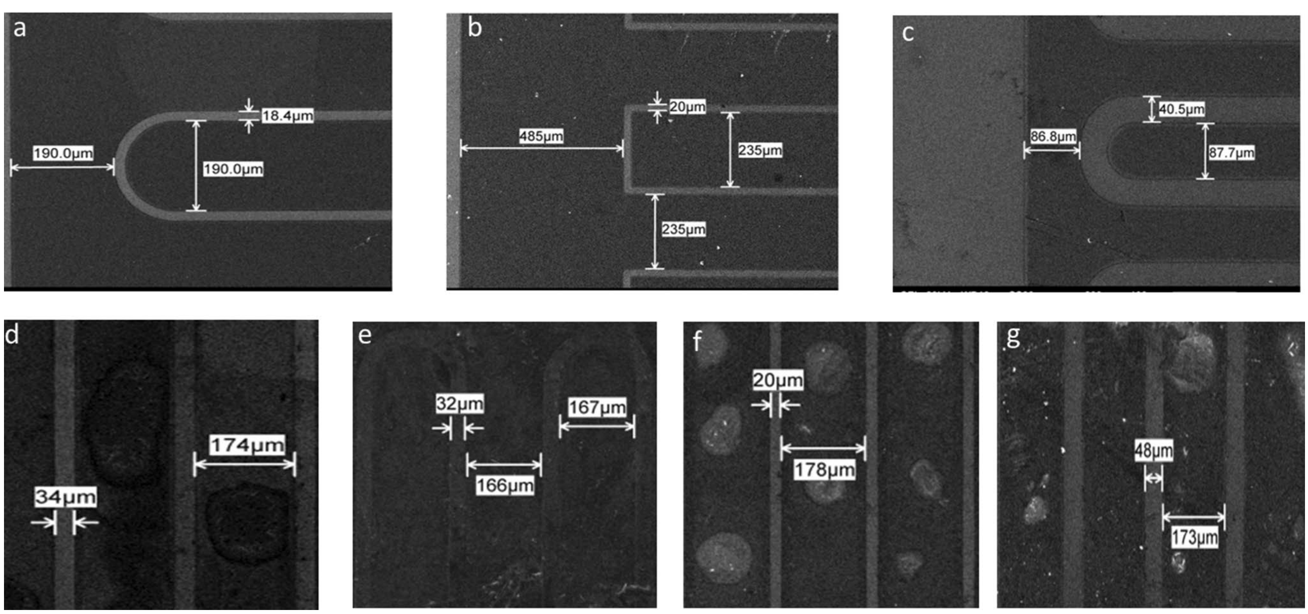

Fig. 6 The surface analysis and dimensions of AlIDEs of different types and structures before and after coated with zinc oxide and different sizes of gold nanorods were determined using scanning electron microscopy (SEM): **a** SEM image of bare 1, **b** SEM image of bare 2, **c** SEM image of bare 3, **d** SEM image of AlIDE after coated with zinc oxide, **e** SEM image of AlIDE after coated with gold nanorod of size 550 nm, **f** SEM image of AlIDE after coated with gold nanorod of size 700 nm, **g** SEM image of AlIDE after coated with gold nanorod of size 980 nm

6.2 Electrical characterizations

6.2.1 I–V characterization of bare AlIDEs

Before the dropping of pH solutions on the active surfaces of the AlIDEs, three devices of different bare were used to test I–V characterization. At 0.7 v, the current variation of bare 1 started at 0.35 μA until it reached 2.5 μA at exactly 2 V as in Fig. 7a. Also at 0.27 v, the current variation of bare 2 started at 0.35 μA until it reached 5 μA at exactly 2 V. Furthermore, at 0.5 V, the current variation of bare 3 started at 0.35 μA until it reached 4.9 μA, at exactly 2 V as in Fig. 7a, respectively. We can conclude that the starting points of variations of the current were all at 0.35 μA, but varied at the end point after reaching 2 V for the devices bare 1, 2, and 3. The results of three bare AlIDEs with I–V characteristics were matched in one graph for easy interpretation of their responses. Based on the response of each device to I–V characterizations, it can be said that the fabrication of the AlIDEs were successful and the devices were able to allow current to pass through them without any short circuit or current leakage, hence, the devices are reliable to be used.

6.2.2 I–V characterization on gold nanorod–zinc oxide composite: pH scouting

After the I–V characterization on the bare AlIDEs, we proceeded to test the devices using different pH solutions, the pH solutions used here were from 1 to 12 and all the solutions have different levels of ions, hence, the abundance of different electrolytes will be in the solution, leads to the changes in the conductivity. The characteristic of I–V curves is presented based on acidic and alkaline media and different fabricated AlIDEs were tested with different pH solutions. The purpose of testing the devices with different pH solutions is based on the mechanism of ion transfer via pH solutions dropped onto AlIDEs surfaces. The graphs of AlIDEs bare and after zinc oxide and gold nanorod deposited describe the influence of the electrolytes on the sensing surface (Fig. 7). The drop of pH solutions covers the desired surface of the AlIDEs with widths and gaps between the finger electrodes. With potential between the aluminum electrodes increases, more ion migration takes place. After the drop of different pH concentrations which ranging from 1 to 12 was dropped on the bare 1 AlIDE, pH 1 and 12 has influence on the device active surface as indicated by Fig. 7b. Also after pH solutions from 1 to 12 were dropped on the bare 2 AlIDE, only pH_1 has much influence on the device active surface as indicated by Fig. 7c. Furthermore, the

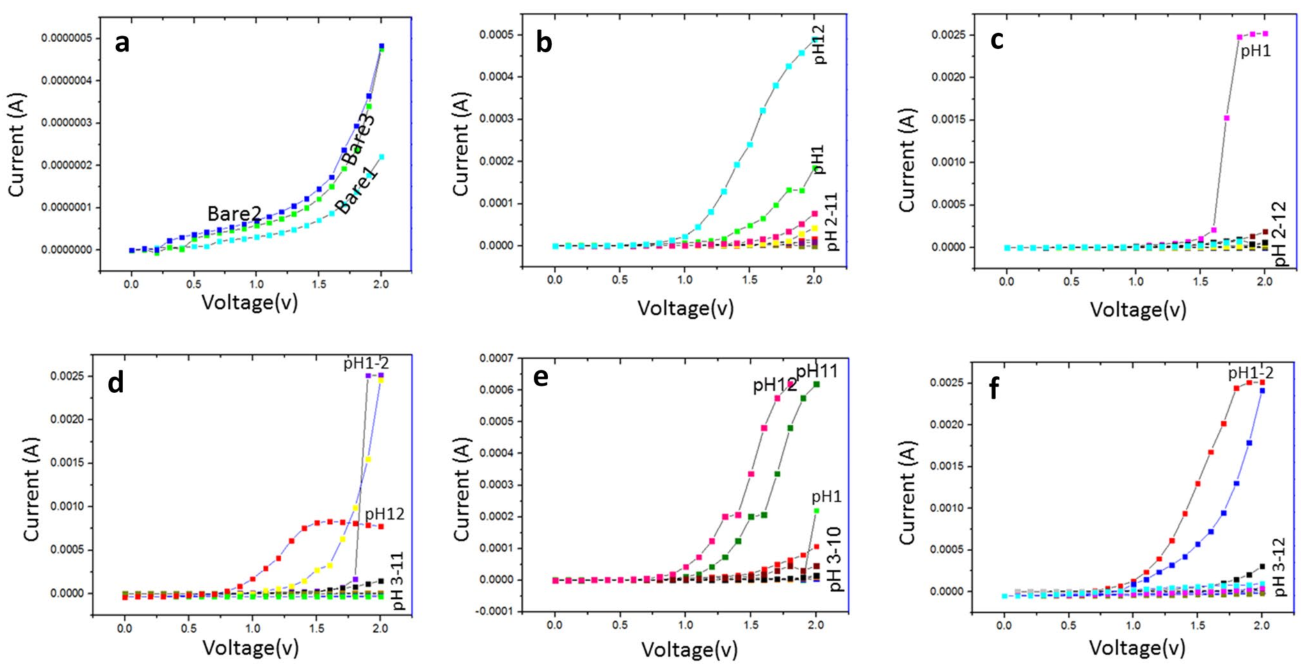

Fig. 7 Electrical characterization of bare AlIDEs and after coated with zinc oxide and gold nanorod using I–V at various pH solutions: **a** Graph of bare 1, 2, and 3 of AlIDES I–V characterization before pH scouting, **b** Graph of bare 1 of AlIDE I–V characterization after pH scouting, **c** Graph of bare 2 of AlIDE I–V characterization after pH scouting, **d** Graph of bare 3 of AlIDE I–V characterization after pH scouting, **e** Graph of AlIDE I–V characterization after coated with zinc oxide with pH scouting, **f** Graph of AlIDE I–V characterization after coated with gold nanorod of size 980 nm with pH scouting

dropping of pH 1–12 on bare 3 AlIDE revealed that pH_1, 2 and 12 has influence on the device as indicated by Fig. 7d. After the device was coated with zinc oxide and followed by pH 1–12 drops, pH 1, 11, and 12 indicated high influences on the device active surface as indicated by Fig. 7e. Last, after the device further deposited with gold nanorod on the zinc oxide and similarly pH solutions pH 1–12 were dropped on the device active surface, pH 1 has indicated a high influence on the device active surface. We can conclude that the bare 1 and 3 have similar response where both acidic and alkaline regions have influence on them. However, bare 2 AlIDE and the device deposited with gold nanorod have similar response in which they have more influence only in acidic regions, it can be said that the deposition of the gold nanorod, brought about a uniform response.

The sensitivity with pH was increased with the levels of electrolytes and this could be improved by the support of conducting substrate with gold nanorod and zinc oxide nanocomposite. The repeatability behavior of the sensors has been compared with different pH solutions tested on without gold nanorod and zinc oxide and with gold nanorods and zinc oxide-coated surfaces. Furthermore, the characteristics of I–V have been appeared to be increased when pH was increased from 1 to 12. Considering the signal without having significant influence on the sensing surface, at acidic range, the response of I–V was appeared to be lower than response of I–V at the alkali range. In other words, response of the bending curves of the I–V at the acidic region is slower than the response of the curve bending at alkali region. The repeated results for pH 1 to 12 indicated the better repeatability and it was observed below 5% to the relative standard deviation (RSD). For pH ranges 1 and 12, the electrode is appropriate for the measurements with electrochemical analysis.

The electrical characterization was done to examine the functionality of the devices after the fabrication and the functionalization steps. As it can be seen clearly, the reproducibility on three bare AlIDEs shows the similar results for all the voltage ranges with minimal differences. Furthermore, all the voltages generated during I–V measurements revealed are comparable and proved that AlIDEs designed with similar parameters and dimensions. Cations of the solution are drawn to the electrode that has a plenty of electrons, while the anions are drawn to the electrode that has a shortage of electrons. The movement of anions and cations in opposite directions within the solution lead to the current generation. The deposition of gold nanorod–zinc oxide nanocomposite has improved the device sensitivity towards the electrical characterization. Although gold-based nanocomposite has attracted much attention in recent decade for biosensing due to its excellent physiochemical properties, it is important to conjugate with novel materials in developing a high-sensitive sensing surface. As presented in the current research, zinc oxide has significant contribution in generating high-performance AlIDE for the excellent electrical characterization. Gold nanorod with high surface area enables the ideal biomolecule functionalization, whereas zinc oxide plays remarkable role in transmitting the electrical signal throughout the electrodes. The applications of zinc oxide as in nanocomposites are widely reported recently. El-Shafai et al. reported the deposition of graphene oxide with zinc oxide nanocomposite in examining the interaction between DNA biomarkers and investigating its drug carrier property in antibacterial analysis. The results justified the ability of the nanocomposite in examining the interaction of human and circulating tumor DNA with the aid of fluorescence spectroscopy [41]. In another study, graphene oxide/zinc oxide nanocomposite was analyzed for impedance measurements. The research concluded that graphene oxide/zinc oxide nanocomposite reveals low loss tangent value and high dielectric permittivity especially in energy storage biosensing applications [42]. Moreover, apart from metals and its oxides, zinc oxides have been conjugated with polymer to create nanocomposites for sensing applications. In a recent work, zinc oxide/polypyrrole nanocomposite was generated for detecting environmental pollutants on solid phase microextracted fiber, where it can detect up to 0.05 µg/L pollutant under optimized conditions [43]. With this regard, the successful application of zinc oxide materials in the presented research is equally acceptable in contrast to other similar zinc oxide materials and its nanocomposites used in detecting biomolecules or other substances, creating high-sensitive biosensing platform. Furthermore, the present research has justified that zinc oxide-based nanocomposite has shown excellent insensitivity towards various electrolytes, thus it is high encouraged to be implemented in developing pH-insensitive biosensors.

6.3 Analysis on Nernst equation and ion movement

The pH is the measurement on molar concentration of hydrogen ions and to understand the mechanism of electrolysis, this study was carried out. The measurement on different pH of a sample was carried out by measuring the potential of that sample in respect to the standard hydrogen. This procedure provides a value of zero for one molar solution of 'H' ions, and therefore, defining the zero of the pH scales. The cell potential for any other values with 'H' ion concentration can be found with the use of Nernst equation:

$$E = E^{\circ} - \frac{RT}{nF} \text{In } Q,$$

where 'E' is the cell potential, 'E°' is the standard cell potential at the temperature of interest, 'R' is the universal gas constant, 'T' is the absolute temperature, 'F' is the Faraday, 'n' is the number of moles of electrons transferred

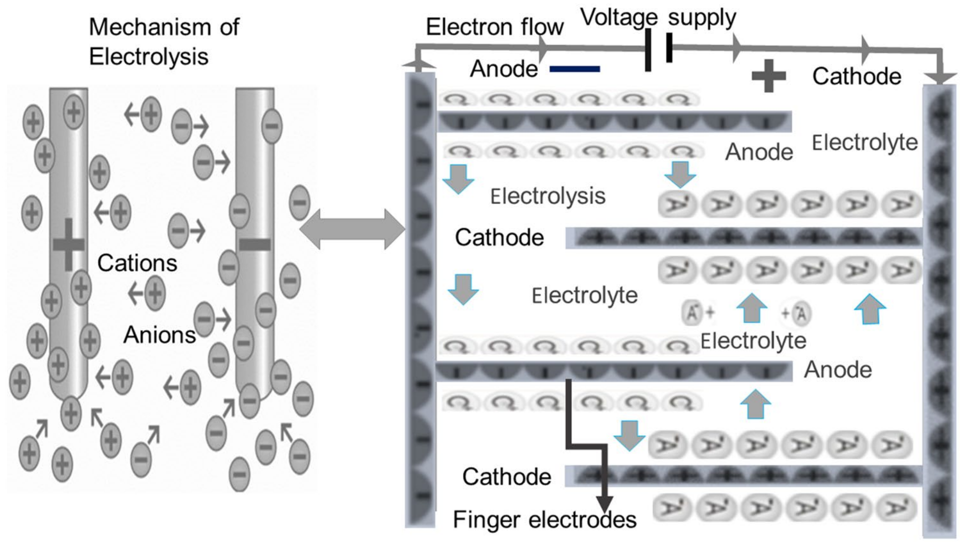

Fig. 8 Mechanism of electrolysis: Electrolysis, process by which electric current is passed through a substance to effect a chemical change. The process is carried out in an electrolytic cell, an apparatus consisting of positive and negative electrodes held apart and dipped into a solution containing positively and negatively charged ions

in the cell reaction or half reaction, and 'Q' is the reaction quotient. Comparison among molar conductance of some common electrolytes is displayed in Table S1.

The common most important characteristic of electrolyte solutions is that they have the ability to convey the electric current and the ability to conduct electricity is dependent on the way of dissolved substance dissociates in the solution in the form of ions. By applying the potential differences to the electrode, the ions can move via the solution as a result of the presence of electric field. The negatively charged ions will move towards the anode and positively charged ions will move towards the cathode (Fig. 8). Furthermore, the neutralization and isolation of ions will take place at the surface of the electrode when the neutral atoms and electrons pass through the circuit [44]. In this perspective, various pH solutions of different values have been used to determine the reaction of the devices at each pH range for the downstream sensing applications.

7 Conclusion

In this study, three different interdigitated electrode (IDEs) sensors based on aluminum serves as a metal contact has been successfully fabricated by a conventional photolithography technique for the purpose of pH sensing and after the fabrication was conducted, gold nanorods and zinc oxide were deposited on the devices as nanocomposite. To determine the sizes of the gaps between the electrodes and also the topological characteristics 3D profiler, SEM, HPM, and AFM were used. The current changes were measured by revealing the micro-electrode sensors using different range of pH solutions. The device fabrication was performed based on the design parameters, which was confirmed by the physical configurations. Electrical properties on bare AlIDE have indicated that the devices are stable in terms of electricity. I–V measurements at various pH values have shown that the aluminum IDEs were well fabricated and are verified to be appropriate as a chemical sensor ideally between the pH ranges of 1 and 12 with all the device fabrications were successful. This information made the foundation for the sensor development with gold- and zinc-based materials to be used on the sensing surfaces.

References

1. C. Cheen, S.C.B. Gopinath, L. Wei, X. Rebecca, V. Perumal, T. Lakshmipriya, M. Shuaib, M. Saheed, Int. J. Biol. Macromol. **116**, 765 (2018)
2. S. Neethirajan, S.K. Tuteja, S.T. Huang, D. Kelton, Biosens. Bioelectron. **98**, 398 (2017)
3. P.S. Kumar, C. Balachandran, V. Duraipandiyan, D. Ramasamy, S. Ignacimuthu, N.A. Al-dhabi, Appl. Nanosci. **5**(2), 169–180 (2015)
4. N.R. Dalila, M.K. Md Arshad, S.C.B. Gopinath, W.M.W. Norhaimi, M.F.M. Fathil, Biosens. Bioelectron. **132**, 248 (2019)
5. S. Taniselass, M.K. Md Arshad, S.C.B. Gopinath, Biosens. Bioelectron. **130**, 276 (2019)
6. H.H. Nguyen, S.H. Lee, U.J. Lee, C.D. Fermin, M. Kim, Materials **12**, 121 (2019)
7. P. Forssén, E. Multia, J. Samuelsson, M. Andersson, T. Aastrup, S. Altun, D. Wallinder, L. Wallbing, T. Liangsupree, M.L. Riekkola, T. Fornstedt, Anal. Chem. **90**, 5366 (2018)
8. N. Bhalla, P. Jolly, N. Formisano, P. Estrela, Essays Biochem. **60**, 1 (2016)
9. P. Ambhorkar, Z. Wang, H. Ko, S. Lee, K.I. Koo, K. Kim, D.I.D. Cho, Micromachines **9**, 1 (2018)
10. H. Li, D. Du, C. Zhu, G. Yang, Y. Lin, Anal. Chem. **87**, 230 (2014)
11. S. Malhotra, A. Verma, N. Tyagi, V. Kumar, Int. J. Adv. Res. Innov. Ideas Educ. **3**, 44 (2017)
12. S. Kiani, P. Rezaei, M. Navaei, M.S. Abrishamian, IEEE Sens. J. **18**, 9971 (2018)
13. C. Wang, L. Yin, L. Zhang, D. Xiang, R. Gao, Sensors **10**, 2088 (2010)

14. H. Gómez-Pozos, J.L. González-Vidal, G.A. Torres, M. de la Luz Olvera, L. Castañeda, Sensors (Switzerland) **14**, 403 (2013)
15. L. Durai, S. Badhulika, New J. Chem. **43**, 11994 (2019)
16. S. Vigneshvar, C.C. Sudhakumari, B. Senthilkumaran, H. Prakash, Front. Bioeng. Biotechnol. **4**, 1 (2016)
17. S. Neethirajan, V. Ragavan, X. Weng, R. Chand, Biosensors **8**, 23 (2018)
18. S. Ramanathan, S.C.B. Gopinath, MK Md Arshad, P. Poopalan, Biosens. Bioelectron. **141**, 111434 (2019)
19. D. Pawar, Microchim. Acta **184**, 253 (2019)
20. Ü. Anik, S. Timur, Z. Dursun, Microchim. Acta **186**, 196 (2019)
21. H. Kaur, A. Bhosale, S. Shrivastav, Int. J. Health Sci. Res. **8**, 315 (2018)
22. N. Soin, S. Norhafiezah, A.H. Azman, M.F. Fatin, U. Hashim, R.M. Ayub, M.A. Farehanim, Adv. Mater. Res. **1109**, 253 (2015)
23. N.S. Mazlan, M.M. Ramli, M.M.A.B. Abdullah, D.S.C. Halin, S.S.M. Isa, L.F.A. Talip, N.S. Danial, S.A.Z. Murad, AIP Conference Proceedings **1885**, (2017)
24. M. Pirsaheb, S. Mohammadi, A. Salimi, M. Payandeh, Microchim. Acta **186**, 231 (2019)
25. L.E. Delle, V. Pachauri, A. Vlandas, M. Riedel, B. Lägel, R. Lilischkis, X.T. Vu, P. Wagner, R. Thoelen, F. Lisdat, S. Ingebrandt, Sens. Actuators B Chem. **265**, 115 (2018)
26. S.C.B. Gopinath, S. Ramanathan, K. Hann Suk, M. Ee Foo, P. Anbu, M.N.A. Uda, MATEC Web of Conferences **150**, 06002 (2018)
27. V. Perumal, U. Hashim, S.C.B. Gopinath, H.R. Prasad, L. Weiwen, S.R. Balakrishnan, T. Vijayakumar, R.A. Rahim, Nanoscale Res. Lett. **11**, 31 (2016)
28. A. Florea, G. Melinte, I. Simon, C. Cristea, Biosensors **9**, 38 (2019)
29. I. Letchumanan, S.C.B. Gopinath, M.K. Md Arshad, P. Anbu, Biosens. Bioelectron. **131**, 128 (2019)
30. D. Tonelli, E. Scavetta, I. Gualandi, Sensors (Switzerland) **19**, 1186 (2019)
31. V. Perumal, M. Shuaib, M. Saheed, N. Muti, J. Chiu, Biosens. Bioelectron. **116**, 116 (2018)
32. L. Coustan, G. Shul, D. Bélanger, Electrochem. commun. **77**, 89 (2017)
33. I. Unlu, J.W. Soares, D.M. Steeves, J.E. Whitten, Langmuir **31**, 8718 (2015)
34. L.L. Sin, M.K. Md Arshad, M.F.M. Fathil, R. Adzhri, M.N.M. Nuzaihan, A.R. Ruslinda, S.C.B. Gopinath, U. Hashim, AIP Conference Proceedings **1733**, 1 (2016)
35. E. Kostal, S. Kasemann, C. Dincer, S. Partel, Multidisciplinary Digital Publishing Institute Proceedings. **2**(13), 2 (2018)
36. D. Sharma, J. Lee, J. Seo, H. Shin, Sensors (Basel). **17**, E2128 (2017)
37. J.D. Benck, B.A. Pinaud, Y. Gorlin, T.F. Jaramillo, PLoS One **9**, e107942 (2014)
38. M.Y. Ho, P.S. Khiew, D. Isa, T.K. Tan, W.S. Chiu, C.H. Chia, Nano **09**, 1430002 (2014)
39. A.K. Muaz, U. Hashim, W.-W. Liu, F. Ibrahim, T. KL, M.S. Mohkta, Appl. Phys. **125**(8), 548 (2016)
40. S. Ramanathan, S.C.B. Gopinath, M.K. Md Arshad, P. Poopalan, F.K. Loong, T. Lakshmipriya, Appl. Phys. A **125**, 548 (2019)
41. N. El-Shafai, M.E. El-Khouly, M. El-Kemary, M. Ramadan, I. Eldesoukey, M. Masoud, RSC Adv. **9**, 3704 (2019)
42. V. Mututu, A.K. Sunitha, R. Thomas, M. Pandey, B. Manoj, Int. J. Electrochem. Sci. **14**, 3752 (2019)
43. H. Amanzadeh, Y. Yamini, M. Moradi, Anal. Chim. Acta. **884**, 52 (2015)
44. G. Serianni, P. Agostinetti, M. Agostini, V. Antoni, D. Aprile, C. Baltador, M. Barbisan, M. Brombin, M. Cavenago, G. Chitarin, M. Dalla Palma, R. Delogu, F. Fellin, N. Fonnesu, N. Marconato, R. Pasqualotto, A. Pimazzoni, E. Sartori, S. Spagnolo, M. Spolaore, P. Veltri, B. Zaniol, M. Zaupa, New J. Phys. **19**, 045003 (2017)

Publisher's Note Springer Nature remains neutral with regard to jurisdictional claims in published maps and institutional affiliations.